Analysis of γ-p Reactions in a Hydrogen Bubble Chamber to 6.0 BeV: Cross Sections and Laboratory Distributions*

CAMBRIDGE BUBBLE CHAMBER GROUP†

Brown University, Providence, Rhode Island, Cambridge Electron Accelerator, Cambridge, Massachusetts, Harvard University, Cambridge, Massachusetts, Massachusetts Institute of Technology, Cambridge, Massachusetts, University of Padova, Padova, Italy, The Weizmann Institute of Science, Rehovoth, Israel

(Received 24 October 1966)

This paper gives an account of the experimental arrangement, the beam properties, and the methods of data analysis for a study of photon reactions in hydrogen at energies up to 6 BeV. The values of cross sections as a function of photon energy are presented for $\gamma+p\rightarrow p+\pi^0$, $\gamma+p\rightarrow n+\pi^+$, $\gamma+p\rightarrow p+\pi^+\pi^-$, $\gamma+p\rightarrow n+\pi^+\pi^+\pi^-$, $\gamma+p\rightarrow p+\pi^+\pi^-\pi^0$, $\gamma+p\rightarrow p+\pi^+\pi^+\pi^-\pi^-$, and $\gamma+p\rightarrow$ (strange particles), as well as a lower limit for the $\gamma+p$ total cross section. In addition, momentum and angular distributions in the laboratory system are given for protons and charged pions from the non-strange-particle reactions.

I. INTRODUCTION

THIS is one of a series of papers reporting the final results of a study of the nuclear interactions of photons with energies up to 6 BeV in a hydrogen bubble chamber. This experiment, recently completed at the Cambridge Electron Accelerator (CEA), constitutes the first comprehensive study of photoproduction in hydrogen above 1 BeV and required considerable adaptation of the usual experimental and analytical techniques. Section II describes the bubble chamber and the special beam transport which created a suitable photon beam. The properties of this photon beam and the method of their determination are given in Sec. III. The unknown energy of the photon responsible for a given event creates special problems in the analysis of the events; the methods used are discussed in Sec. IV. The cross sections for reactions involving "stable" particles with various multiplicities are presented in Sec. V, and Sec. VI. reports a number of observed (laboratory) momentum and angular distributions.

Special reactions such as production of ρ mesons,[1] isobars,[2] ω mesons,[3] and strange particles[4] are discussed fully in the other papers of this series. Some preliminary reports of this work have appeared.[5]

II. EXPERIMENTAL ARRANGEMENT

The hydrogen bubble chamber was 12 in. in diameter and 6 in. deep. It was originally built at Columbia University and has been described elsewhere in detail.[6] It was transferred in 1962 to the MIT Laboratory for Nuclear Science, and was modified for this experiment at the CEA. The thickness of the aluminum beam window was reduced to $\frac{1}{16}$ in. The window size was 2.5 in. by 4.0 in. The chamber was located in a magnetic field of 13.2 kG and exposed to a hardened, well-collimated bremsstrahlung beam of maximum energy up to 6 BeV.

The beam used in this experiment contained approximately 50 equivalent quanta per pulse. The shape of the beam, and this low intensity, helped to prevent the obscuring of interaction vertices by electrons from pair production in the entrance window of the chamber and in the bubble-chamber liquid itself.

To achieve a low-intensity beam while maintaining the high-intensity circulating beam in the accelerator, for stable operation and compatibility with other simultaneous beam users, the double conversion arrangement shown in Fig. 1 was used. The circulating electron beam spilled onto a $\frac{1}{10}$ radiation-length-thick internal tungsten target, producing a high-intensity

* This work is supported in part through funds provided by the U. S. Atomic Energy Commission and by the Istituto Nazionale di Fisica Nucleare, Italy.

† Group members (by institution) are: H. R. Crouch, Jr., R. Hargraves, B. Kendall, R. E. Lanou, A. M. Shapiro, M. G. Taylor, and M. Widgoff, Brown University, Providence, Rhode Island; G. E. Fischer, Cambridge Electron Accelerator, Cambridge, Massachusetts; C. A. Bordner, Jr., A. E. Brenner, M. E. Law, U. Maor, T. A. O'Halloran, Jr., F. D. Rudnick, K. Strauch, J. C. Street, and J. J. Szymanski, Harvard University, Cambridge, Massachusetts; P. Bastien, B. T. Feld, V. K. Fischer, I. A. Pless, A. Rogers, C. Rogers, E. E. Ronat, L. Rosenson, T. L. Watts, and R. K. Yamamoto, Massachusetts Institute of Technology, Cambridge, Massachusetts; G. Calvelli, F. Gasparini, L. Guerriero, J. Massimo, G. A. Salandin, L. Ventura, C. Voci, and F. Waldner, University of Padova, Padova, Italy; A. Brandstetter, Y. Eisenberg, and A. Levy, The Weizmann Institute of Science, Rehovoth, Israel.

[1] Cambridge Bubble Chamber Group, Phys. Rev. **146**, 994 1966).

[2] Cambridge Bubble Chamber Group (to be published).

[3] Brown-Harvard-MIT-Padova-Weizmann-Institute Bubble Chamber Group, Phys. Rev., this issue, **155**, 1468 (1967).

[4] Cambridge Bubble Chamber Group, Phys. Rev. (to be published).

[5] H. R. Crouch *et al.*, Phys. Rev. Letters **13**, 636 (1964); **13**, 640 (1964); in *Proceedings of the International Symposium on Electron and Photon Interactions at High Energies*, edited by G. Hohler *et al.* (Deutsche Physikalische Gesellschaft, Hamburg, 1965), Vol. II, p. 1; in *Proceedings of the Second Topical Conference on Resonant Particles* (Ohio University Press, Athens, Ohio, 1965), p. 476.

[6] F. Eisler *et al.*, Nuovo Cimento **10**, 468 (1958).

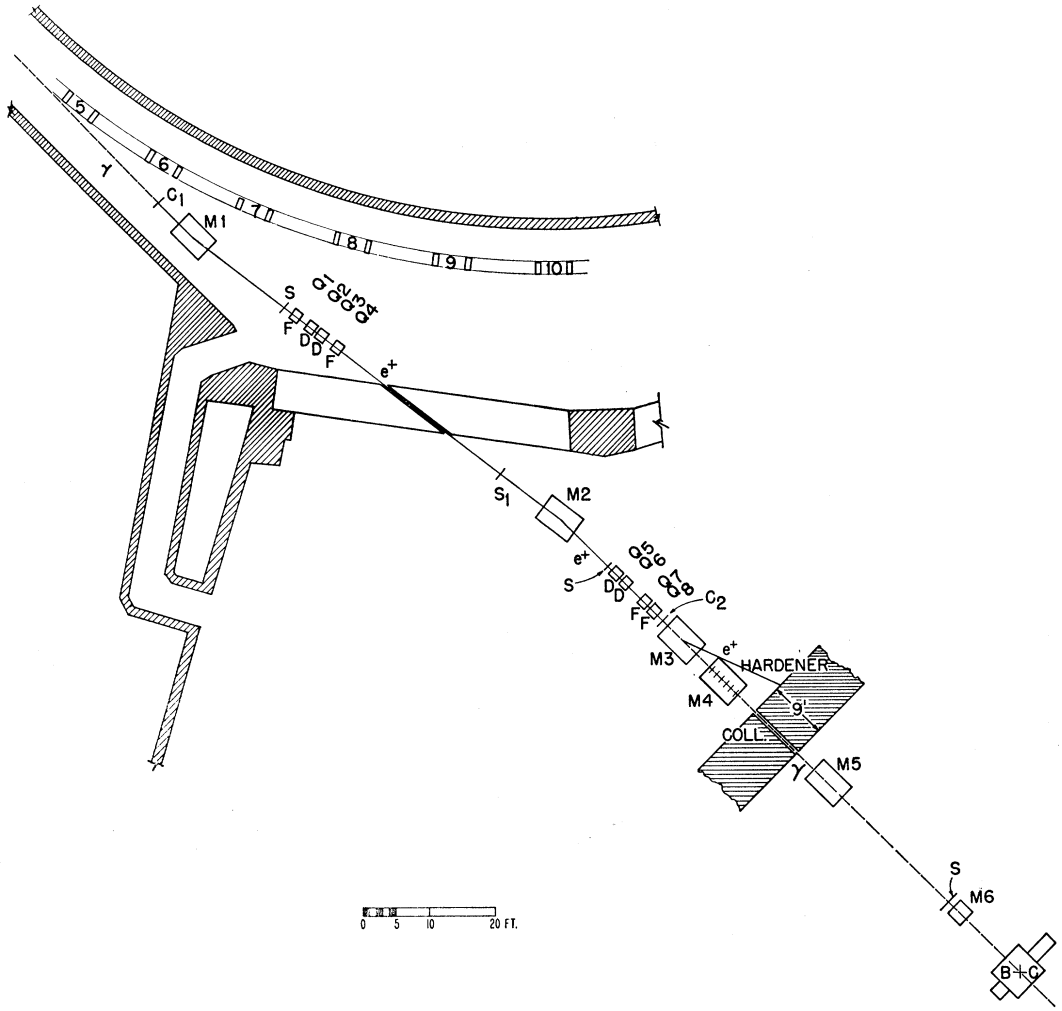

FIG. 1. The experimental arrangement on the floor of the Cambridge Electron Accelerator. The spaced beryllium hardener is indicated by M4 and the bubble chamber by B. C.

bremsstrahlung beam. This photon beam was converted into electron-position pairs at C1, which was a copper converter $\frac{1}{2}$ in. by $\frac{1}{2}$ in. perpendicular to the beam, whose thickness was variable by remote control from $\frac{1}{2}$ in. to $\frac{1}{64}$ in. The positrons were then momentum selected by a standard 72-in. bending magnet M1 and focused by 4-in.-diam quadrupoles Q_1—Q_4 onto the $\frac{1}{2}$-in. slit S1 outside the main shielding wall of the accelerator. This positron beam passed through a second bending magnet M2 and a further set of quadrupoles Q_5—Q_8 to C2, a second converter similar to C1 and located in front of clearing magnet M3. These positrons, if allowed to pass through the bubble chamber, would be a beam of the desired size. Since the gamma rays produced at C2 essentially follow the path of the positrons, the desired gamma-ray beam was produced in the chamber. The resulting low-intensity bremsstrahlung beam from C2 was hardened by passing it through 1.8 radiation lengths of beryllium, composed of 1-in.-thick slices distributed uniformly along the 72-in. length of magnet M4. The hardened beam was collimated and passed through clearing magnets M5 and M6 before entering the bubble chamber. Additional slits, positioned as shown in Fig. 1, aided in producing a clean beam, and in addition the double bend introduced by magnets M1 and M2 ensured that neutral particles orginating in the vicinity of the main accelerator target could not enter the bubble chamber.

The purpose of the hardener is to reduce the relative intensity of the very low-energy photons by absorption through the Compton scattering processes. This reduces the number of Compton recoil electrons in the chamber relative to the number with an unhardened beam, allowing exposure to a larger photon flux through the chamber. However, the hardener also converts some high-energy photons into e^+—e^- pairs; it was distributed

in slices in M4 rather than as a compact segment in order to reduce the probability of radiation in the direction of the chamber by the members of these pairs.

The effect of distributing the hardener was studied by comparing the energy spectra of photons for beams with the same maximum energy (5.0 BeV) passed through compact and distributed hardeners. The spectra were normalized to the same number of photons above 3.0 BeV, where little of the secondary radiation is expected to occur. The ratio of number of photons obtained with the distributed hardener to the number of photons obtained with a compact hardener was found to be 0.75 ± 0.06 and 0.78 ± 0.07, in the intervals 0.1–1.5 and 1.5–3.0 BeV, respectively. From this we conclude that distributing the hardener along the beam in a magnetic field does significantly reduce the secondary radiation in the chamber.

The maximum energy of the photon beam was set primarily by the energy of the circulating electron beam (which varied between 4.75 and 6 BeV to accommodate other users), and secondly by the selected energy of the positron transport system. The intensity of the beam could be controlled by varying the positron beam energy or by varying the thickness of C1 or C2. The usable photon intensity was limited by the background of pairs produced in the liquid of the chamber and in the $\frac{1}{16}$-in. aluminum beam window of the chamber. Typically the positron transport system would be set at an energy within 50 MeV of the machine energy and C1 and C2 would be set at $\frac{1}{10}$ of a radiation length. Such an arrangement yielded a photon flux at the bubble chamber of approximately 50 equivalent quanta per picture, producing an average of 4 electron-positron conversion pairs in the liquid and an equal number in the beam window.

III. THE PHOTON BEAM

The geometric properties of the photon beam have been determined experimentally by measuring the density and direction of electron-positron pairs produced in the liquid of the chamber. As summarized in Fig. 2, the horizontal and vertical widths were approximately 5 cm and 9 cm and the dip (θ) and azimuthal (ϕ) angular spreads were 0.4° and 0.2°, respectively.

The momenta of about 30 000 pairs were measured to obtain the energy distribution of the photon beam in the chamber. In order to normalize the spectrum obtained from these measurements to the total amount of energy in the data, a count of pairs was made at uniform intervals throughout the film and an average number of pairs per picture was calculated. In these calculations no pairs with energy less than 4 MeV were used as the scanning efficiency for detecting pairs close to this minimum is uncertain. In order for the normalization procedure to be correct, this efficiency must be the same for pairs selected for measurement as for all the pairs that are counted. We have shown that these

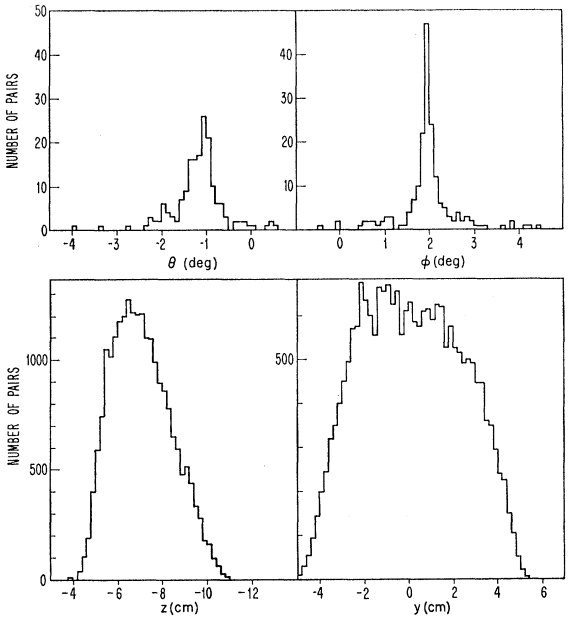

FIG. 2. The spatial and directional distributions of e^+e^- pairs in the bubble chamber. The coordinate system used is oriented so that the horizontal z axis lies along the axis of the bubble chamber, normal to the front glass and directed toward the cameras; the x axis is horizontal and roughly along the beam direction and the y axis is vertical. The angle φ is the angle between the projection on the x-y plane and the x axis; the angle θ is the dip angle (90 deg minus the angle with the z axis).

two efficiencies are the same by measuring all pairs counted on a subsample of film, thus eliminating the need for normalization in this sample. The resulting spectrum agreed, within experimental uncertainties, with that found by the normalization technique.

The normalized pair-energy spectrum is converted to a photon-energy spectrum by using a theoretical pair-production cross section. This cross section was found by numerical integration of the coherent and incoherent differential cross sections, with screening corrections, as given by Wheeler and Lamb.[7] In addition, a 2.7% correction for molecular screening[8] and a 0.93% radiation correction[9] were made.

Figure 3 shows the photon-energy spectrum derived by the method indicated above. Only statistical errors are shown; a systematic uncertainty of less than 5% also exists as a result of uncertainties in the normalization of pair spectra to pair counts.

A total of about 5 nuclear events have been seen which appear to occur on target nuclei other than protons. We expect, then, that some of the pairs used determine the flux also occurred on nonhydrogen targets and estimate this contamination to be no more than about 5%.

[7] J. A. Wheeler and W. E. Lamb, Jr., Phys. Rev. **55**, 858 (1939); **101**, 1836 (1956).
[8] D. Bernstein and W. K. H. Panofsky, Phys. Rev. **102**, 522 (1956).
[9] K. Mork and H. Olsen, Phys. Rev. **140**, B1661 (1956).

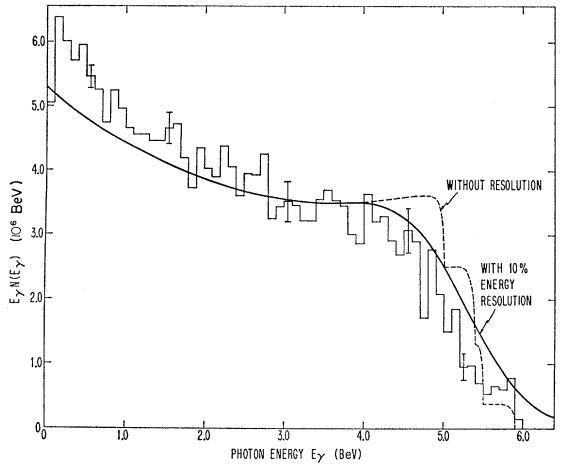

FIG. 3. The photon-energy distribution for the sample of events shown in Figs. 4–11. The solid and dashed curves are sums of appropriately weighted bremsstrahlung distributions with and without a 10% energy resolution, respectively. This weighting is due to the fact that the experiment was not performed at a unique positron energy but rather at several positron energies. The theoretical curves are normalized to the energy above 0.1 BeV. Errors shown are statistical.

Also shown in Fig. 3 is a theoretical distribution that is the sum of thin-target spectra for our beam energies weighted according to the total energy flux at each energy. An estimated 10% energy resolution is included and the curve is normalized to the same total energy as the experimental distribution above 0.1 BeV. The actual distribution is close to that expected for bremsstrahlung except for some depletion at high energies and an enhancement at lower energies, which may be attributed to the hardener. The depletion of those photons of energies that contribute to Compton scatterings is indicated in the first bin on Fig. 3.

IV. ANALYSIS OF EVENTS

A total of 865 000 pictures were scanned to obtain the sample of events analyzed. All events with three or more prongs, or a single prong with one or two V^0's, were recorded; in addition, 93 500 pictures were scanned for single-prong events. The beam intensity used yielded about one event per 100 pictures, not counting the single-prong events.

The spatial reconstruction of tracks and the testing of kinematic hypotheses were done with the CERN programs, THRESH and GRIND, respectively. Except for the single-prong sample, events were accepted in a fiducial volume beginning 1.5 cm inside the beam window and extending 17.75 cm long along the beam direction; this insured a sufficient track length for good measurements in all cases. Since there was poor scanning efficiency of the single-prong sample close to the beam window, for these events the fiducial volume began 4.25 cm inside the beam window. The interaction types considered in the kinematic analysis are included in the list given in Table I. (In the remainder of the paper reactions will be numbered according to the scheme of Table I.) We first describe the analysis of the nonstrange events with more than one prong, then the strange-particle events, and, finally, the single-prong events.

The Three-Constraint Sample

The average direction, but not the energy, of the incident photon beam is known; therefore, testing a hypothesis with no missing neutral particle involves a fit with three constraints (3C). The χ^2 distribution obtained when such fits were attempted for a random sample of three-prong events is shown in Fig. 4. On the basis of this distribution a separation between events without a missing neutral and the remainder was made by setting a maximum χ^2 of 10 to define 3C events.

Four events were ambiguous between pK^+K^- and $p\pi^+\pi^-$ interpretations. These were included in the $p\pi^+\pi^-$ sample and constitute a negligible contamination. Twenty-three events were ambiguous betwen pK^+K^- and $p\pi^+\pi^-\pi^0$ or $n\pi^+\pi^+\pi^-$. These were placed in a special strange-particle category and will be discussed in the paper on strange particles.

Another small contamination arises from 0C events in which the π^0 is emitted within 5° of the beam direction. Such events may satisfy the 3C kinematics. This contamination was studied by comparing the relative number of charged and neutral pions produced at less than 5° in the $p\pi^+\pi^-(x\pi^0)$ events and this contamination was calculated to be less than 0.5% in reaction (3). This assumes a similarity in the angular distribution for the charged and neutral pions.

TABLE I. Types of events and number of each found in 865 000 pictures.

Reaction	No. of events	No. ambiguous[d]
(1) $p\pi^0(+x\pi^0)$[a]	871[c]	
(2) $n\pi^+(+x\pi^0)$[a]	947[c]	
(3) $p\pi^+\pi^-$	4425	
(4) $p\pi^+\pi^-(+x\pi^0)$[b]	1592	172
(5) $n\pi^+\pi^+\pi^-(+x\pi^0)$[a]	583	
(6) $p\pi^+\pi^+\pi^-\pi^-$	134	
(7) $p\pi^+\pi^+\pi^-\pi^-(+x\pi^0)$[b]	82	26
(8) $n\pi^+\pi^+\pi^+\pi^-\pi^-(+x\pi^0)$[a]	50	
(9) Seven-prong events	5	
(10) Strange particles	170	36
(11) Unassigned (three-prong)	135	
(five-prong)	25	
(V^0 events)	6	

[a] $x=0, 1, 2, \cdots$.
[b] $x=1, 2, 3, \cdots$.
[c] The sample of one-prong events are obtained from a subsample of 93 500 pictures.
[d] Ambiguous events are events where no decision was possible on the basis of kinematics and ionization between two or more reaction types. Unassigned events are events which did not satisfy the criteria for assignment to any reaction type.

The Zero-Constraint Sample

All events that do not satisfy a 3C hypothesis will satisfy hypotheses that include a missing neutral particle. In order to solve the kinematic equations in this case, a value for the missing mass must be assigned; when this is done, the system of equations is just determined and a solution can be calculated. Therefore, these events constitute the 0C sample. Since any missing mass yields a solution, this kinematic calculation cannot distinguish from one another events with a neutron, a π^0, or multiple neutrals. Only the neutron and π^0 masses were included as missing masses in the standard hypotheses that did not involve strange particles. It is important to note that different missing-mass assumptions produce solutions with different calculated values for the energy of the incident photon.

A choice between the neutron and π^0 hypotheses for the 0C events was made by comparing the predicted and observed bubble densities of the track that was ambiguous between a proton and a π^+. Application of bubble density tests did not resolve the ambiguity in some of the 0C events and these are listed in Table I as *ambiguous* events. We have made an exception in the case of ambiguity between a K and a π meson hypothesis for a track in a 0C event where no V^0 is seen. In this case, the pion hypothesis was chosen, based on the observation that the cross section for pion-pair production is much larger than that for strange-particle production.

The loss of 0C events from reaction (4) to reaction (3) has been discussed. While it represents less than 0.5% of a contamination to reaction (3), it is less than a 3% loss to the 0C reactions. Thus, in considering the whole sample, the effect has been negligible; however, in the study of some particular processes, such as ω production, it could be relatively large and further studies carried out in these cases are presented in the papers discussing the specific processes.

An obvious consequence of the lack of knowledge of the incident photon energy is that a given event with more than one missing neutral cannot be distinguished in the 0C sample and, therefore, such events contaminate the samples of assumed neutron or single π^0 events. It is clear that the test of bubble density cannot distinguish such events, since the momenta and masses of the charged particles are not changed by assuming the wrong missing mass. In addition, when a true multiple-neutral-particle reaction is analyzed as a single-neutral-particle event, the calculated photon energy is lower than the true value. Therefore, in order to measure the cross section as a function of energy for the single-neutral-particle reaction, the multiple neutral contamination to the 0C sample must be estimated.

This has been done for the 0C subclass of reaction (4) and (5) by a statistical procedure, based on the observation that the distribution of laboratory production angles for the assumed neutral particle in events

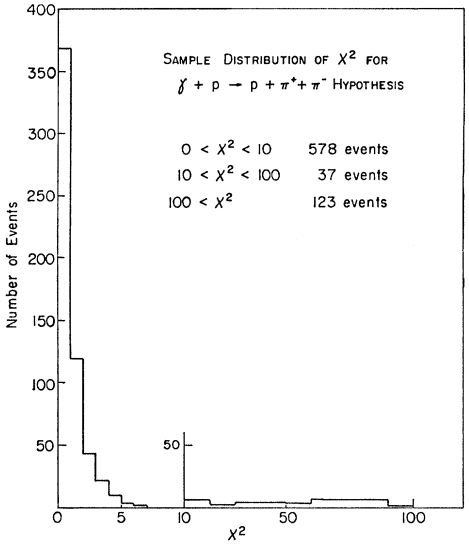

Fig. 4. The distribution of χ^2 values for a random sample of three-prong events when fitted to a 3C hypothesis. A maximum value of 10 was used in selecting events for the 3C sample.

with missing neutrals differs from that for corresponding charged particles. No dominating unstable particle is observed in reaction (6) which might account for this difference. Our statistics do not warrant this procedure for the higher-order reactions, (7) and (8).

The procedure followed in estimating the amount of contamination was to perform a least-squares fit to the observed neutral angular distribution by a superposition of distributions assumed to represent: (1) the true single neutral events and (2) the multiple neutral events analyzed as if only one neutral were produced. Events in which final-state interactions were evident [such as the production of η or ω mesons in reaction (4)] were removed. However, it was found that these omissions produced no significant change in the conclusions.

We first note the empirical fact that the shapes of the laboratory angular distributions of charged pions in reactions (4), (6), and (7) are very similar. This is shown in Fig. 5. This is the case in spite of the differing multiplicities of pions and photon-energy distributions for these reactions. We therefore feel justified in assuming that the distributions of single neutral pions is the same in the 0C events and use, for neutral pions from the single neutral events, the distribution of charged pions in reaction (4).

An examination of the angular distributions of protons in reactions (4), (6), and (7) shows much poorer agreement so that reaction (5) (neutron events) could not legitimately be analyzed by the process used for reaction (4). We consider these neutron events after describing the analyses of the π^0 events.

The angular distributions of the multiple neutral events (analysed as single π^0 events) contaminating the

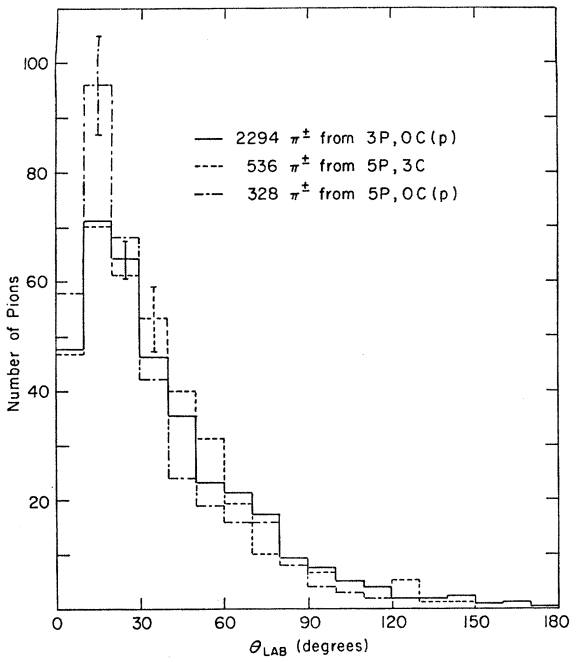

FIG. 5. Laboratory angular distributions of charged pions in reactions (4), (6), and (7). The distributions are normalized to 360 events each to allow the shapes to be compared easily.

sample is estimated by reanalyzing the 5-prong, 3C [reaction (6)] sample as 3-prong, 0C events, deleting a pair of pions to simulate two missing π^0's. Higher multiplicities of missing neutrals were simulated using the 5-prong, 0C sample [reaction(7)] as above. Since the shapes of the distributions were very similar we cannot estimate the fraction arising from events with more than two missing neutral particles.

Figure 6 shows the various distributions used to estimate the contamination. The angular distribution of the neutral pion in the uncorrected 3-prong, 0C sample [reaction(4)] is shown in Fig. 6(a). Figures 6(b) and 6(c) show the component distributions: in Fig. 6(b), the charged-pion distribution from reaction (4) which simulates the single-π^0 distribution and in Fig. 6(c), the single-π^0 distribution as generated from the reanalyzed events of reaction (6). The best-fit combination appears in Fig. 6(d). This analysis allows us to estimate the fraction of single-π^0 events in the 3-prong, 0C proton sample at 0.53 with the 90% confidence limits at 0.43 and 0.63.

A similar procedure could not be applied to the neutron, 3-prong, 0C sample because the proton distributions varied too widely to allow simulation of the single-neutron distribution from them with any confidence. Using the different proton distributions yielded estimates for the fraction of neutron-only events ranging from 40% to 90%. We note that this is consistent with the fraction of single π^0's in the proton sample and, considering the similarity of the problem in the two samples, we use the same estimate of 0.53 for the fraction of neutron-only events in the 3-prong, 0C, neutron events.

In order to estimate cross sections for reactions (4) and (5), we assume that all contaminations of these reactions arises from events with two missing neutrals possessing the photon energy dependence of the 5-prong, 3C events [reaction (6)]. We then use the photon-energy distribution which results when these are analysed as 3-prong, 0C events as the energy distribution of the contamination. This distribution, normalized to the amounts of contamination indicated above, is subtracted from the distribution of 3-prong, 0C events before a cross section is calculated.

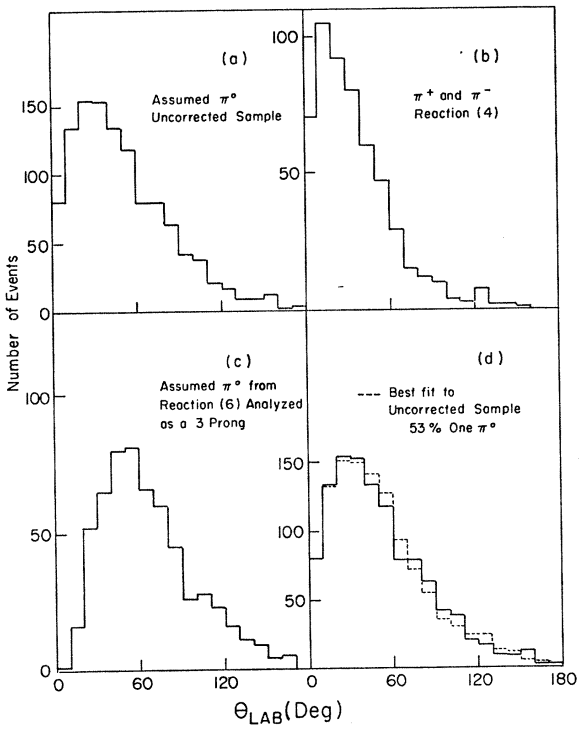

FIG. 6. Laboratory angular distributions used in analysis of multiple-π^0 contamination in reaction (4); (a) for assumed π^0 in uncorrected sample, (b) for π^+ and π^- in reaction (4), and (c) for assumed π^0 in reaction (6) when analyzed as three-prong event. The best fit of (b)+(c) to (a) is shown in (d) as the dashed histogram. This best fit yields 53% single π^0 and 47% more than one π^0.

Strange-Particle Sample

The strange-particle sample included events with one or more visible V^0 decays, events with a charged-particle decay, and events without visible decay. All the events of the first and second classes were assigned to an event type on the basis of kinematic fit and bubble density determination. If there was a 3C fit with χ^2 less than 10 which was consistent with the bubble-density determination, this was taken. If not, then the

0C fit or fits consistent with the bubble-density determination were accepted.

Those events without a visible decay which, however, fit kinematically a hypothesis involving strange particles, were not taken as strange-particle events unless one or more charged strange particles could be positively identified on the basis of bubble-density determination. For convenience in calculation of corrections a cutoff of 600 MeV/c in meson laboratory momentum was imposed on events fitting a hypothesis with a single charged K meson, and 800 MeV/c on events with two charged K mesons. Events in which the meson momenta were higher were arbitrarily placed in the appropriate pion samples. Again if there was a 3C fit with χ^2 less than 10 which was consistent with the bubble-density determination, this was taken. If not, then the 0C fit or fits consistent with the bubble density determination were accepted.

Single-Prong Sample

The single-prong events were subject to a 0C fit only. In many cases this led to a unique agreement with either the $p\pi^0$ or the $n\pi^+$ hypothesis [reactions (1) and (2)]. In those cases where both hypotheses agreed kinematically with what was observed, bubble-density estimates permitted a unique choice in all cases.

The $p\pi^0$ sample was contaminated by low-energy neutron-proton scatterings, arising from beam contamination, which when analyzed as $p\pi^0$ events resulted in a low-momentum peak in the proton-momentum distribution. Events of this type were found throughout the chamber, outside as well as inside the volume containing the photon beam. They were kinematically consistent with proton recoils from low-energy neutrons. Their spatial distribution was consistent with the assumption that they were uniformly distributed throughout the chamber. The distribution of the events outside the beam volume was used to correct the distributions of the events inside the beam volume assuming a uniform distribution. This correction was 13% of the total sample of proton events. There was no contamination of the $n\pi^+$ sample by neutron-induced events.

The contamination of the single-prong samples by γ-p (Compton) scattering is negligible. The contamination by events with more than one neutral (which might be important for $E_\gamma > 0.5$ BeV) could not be simply estimated and the statistics of the samples did not seem to warrant an elaborate analysis.

Other Contamination and Bias

The contamination of the entire sample by neutron-induced events is estimated at less than 0.3% for all except single-prong, proton events. This was determined by attempting the kinematic analysis of a sample of three-prong, 3C events on the assumption of an incident neutron. Also no three-prong, five-prong, or strange-particle events were found which orginated outside the beam volume.

In order to test for bias in the reconstruction and fitting programs, the masses of a sample of K^0 and Λ^0 decays were computed without constraints. Values of 507±8 MeV for the K^0 and 1117.1±0.5 MeV for the Λ^0 (the errors given are statistical) were obtained. Thus there is no evidence for any large, systematic error in calculated mass values. Another check on possible bias is obtained from measured masses of the ω and N^* resonances. These are found to be 786±2 MeV for the ω and 1225±15 MeV for the N^*, in good agreement with accepted values.

Also included in Table I are classes of *unassigned* events. These are events that were either unmeasurable or failed to satisfy any kinematic hypothesis. The unmeasurable events were generally identifiable but no quantitative information is available for them. We consider the number of such events indicated in Table I to be small enough to justify neglecting them.

V. CROSS SECTIONS

The cross sections shown in Figs. 7 through 10 have been corrected for a (97.0±1.0)% scanning efficiency for nuclear events except for the single-prong samples,

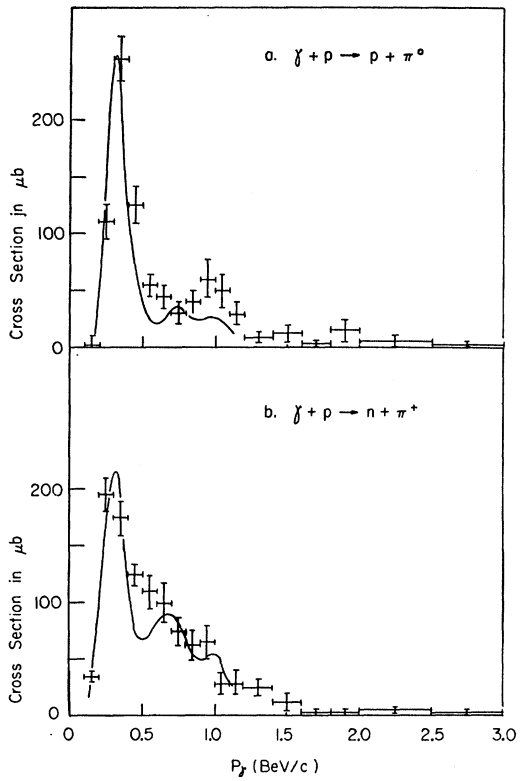

FIG. 7. Observed cross sections for single-prong events interpreted as due to single-pion production, corrected for neutron background. The solid curves are the results of previous counter measurements (see Ref. 10). (a): $\gamma p \to p + \pi^0$; (b): $\gamma p \to n + \pi^+$.

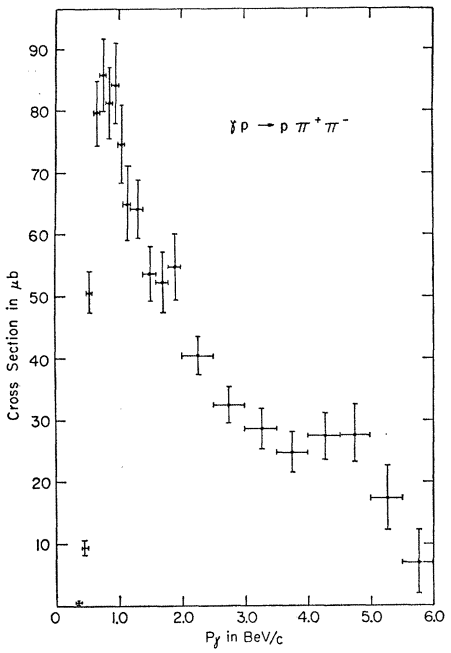

FIG. 8. Cross section for $\gamma p \rightarrow p+\pi^+ +\pi^-$.

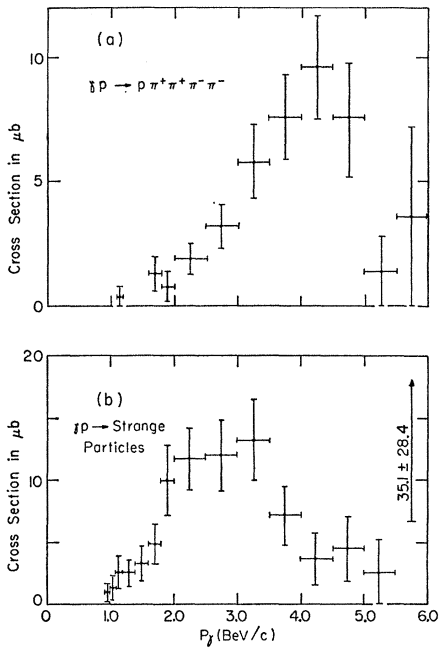

FIG. 10. Cross sections for (a) $\gamma p \rightarrow p+\pi^+ +\pi^- +\pi^-$ and (b) strange-particle events. The strange-particle cross section has been corrected for neutral decay modes and potential path.

which were double scanned and for which the scanning efficiency was $(99.4\pm0.3)\%$. The uncertainties shown include the statistical uncertainty of the sample of events, the statistical uncertainty of the sample of pairs from which the photon spectrum was calculated, the uncertainty in the scanning efficiency, and any uncertainties arising from special problems with the individual samples which will be discussed below. Not included is the possible 5% uncertainty in photon flux due to events on nonhydrogenic atoms or the 5% uncertainty in the absolute normalization of the photon spectrum mentioned in Sec. III.

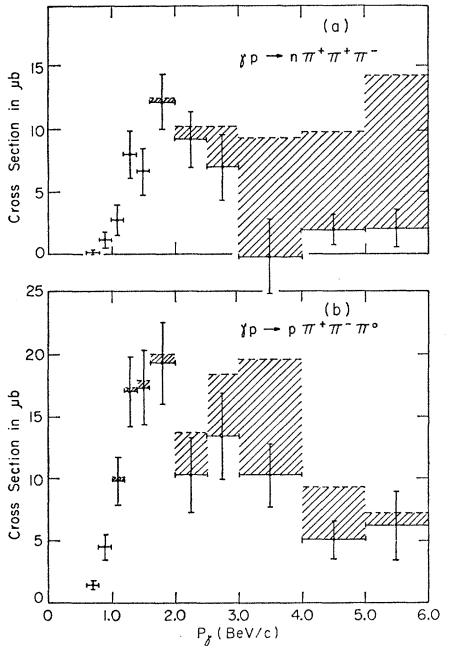

FIG. 9. Cross sections for (a) $\gamma p \rightarrow n+\pi^+ +\pi^+ +\pi^-$ and (b) $\gamma p \rightarrow p+\pi^+ +\pi^- +\pi^0$. The shaded regions are the upper and lower limits for the central value. See discussion of Fig. 9 in text.

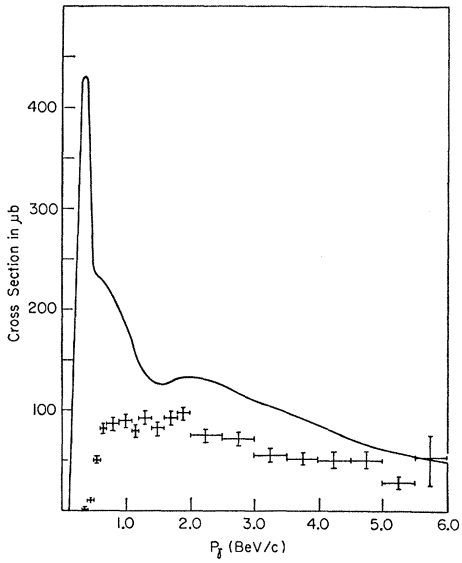

FIG. 11. The points represent the cross section which the chamber allowed us to calculate unambiguously, giving a lower limit to the total cross section. The solid curve is the outline of the cross section for all events, including single prongs, for which a nominal or definite photon-momentum assignment could be made. See text.

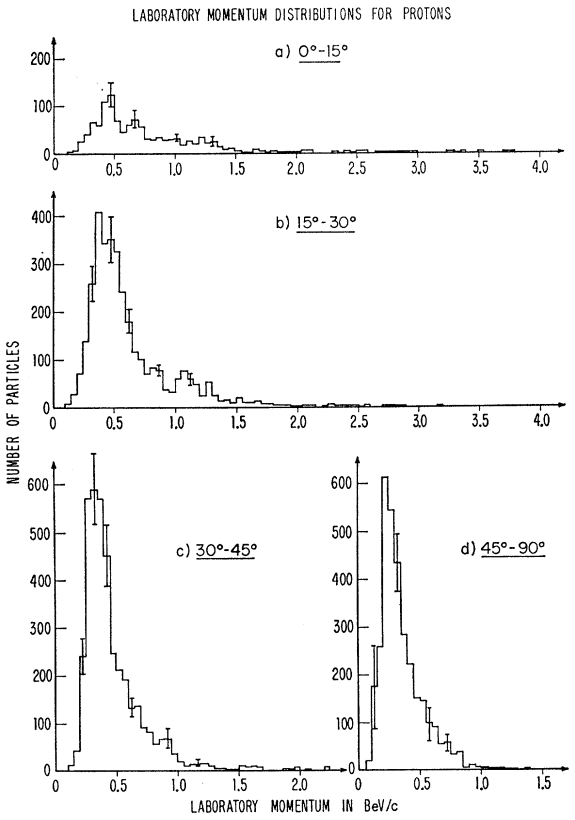

FIG. 12. Laboratory momentum distributions of protons in intervals of 50 MeV/c for various regions of proton laboratory emission angles.

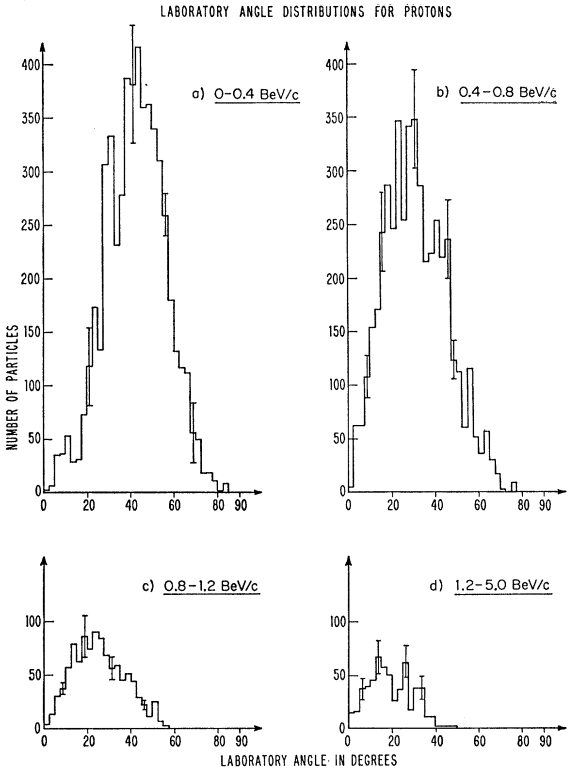

FIG. 13. Laboratory angular distributions of protons in intervals of 2.5 deg for various regions of proton laboratory momenta.

Fig 7 shows the cross sections for the single-prong events interpreted as

$$\text{(a)}\quad \gamma p \rightarrow p+\pi^0$$

and

$$\text{(b)}\quad \gamma p \rightarrow n+\pi^+$$

as a function of photon momentum. The $\gamma p \rightarrow p+\pi^0$ cross section has been corrected for background as discussed in Sec. IV and the estimated uncertainty of this subtraction is included in the uncertainties shown. Neither cross section has been corrected for contamination by events in which multiple neutrals are produced. The results agree within the uncertainties with the results of the Aachen–Berlin–Bonn–Hamburg–Heidelberg–München bubble-chamber collaboration.[10,11] The results of previous counter measurements[12] are also shown in Fig. 7 by the solid curves. Below 0.4 BeV, where the contribution from multipion production is negligible, the agreement is excellent. Above 0.5 BeV, processes involving more than one neutral product can become important and the interpretation of single-prong events as single-pion production can no longer be considered reliable. This is indicated by the discrepancies between our results and the counter measurements at higher energies.

Figure 8 shows the cross section for the reaction $\gamma p \rightarrow p\pi^+\pi^-$. Figure 9 gives the cross sections for the reactions $\gamma p \rightarrow p\pi^+\pi^-\pi^0$ and $\gamma p \rightarrow n\pi^+\pi^-\pi^+$. Since these latter reactions correspond to zero constraint kinematical fits, a given event could frequently be fit by both hypotheses. As previously discussed, if ionization measurements did not allow a decision, the event was classified as ambiguous. A point with an error bar in each case is the cross section when the ambiguous events are not included in the sample. Hence these points represent a lower limit to each cross section. These lower limits to the cross section have been corrected for contamination by events in which multiple neutrals

[10] Aachen-Berlin-Bonn-Hamburg-Heidelberg-München Bubble Chamber Collaboration, Nuovo Cimento **41**, 270 (1966).

[11] Aachen-Berlin-Bonn-Hamburg-Heidelberg-München Bubble Chamber Collaboration, DESY 66/32, 1966 (unpublished); also contributions to the International Conference on High-Energy Physics, Berkeley, 1966 (unpublished).

[12] G. Källén, *Elementary Particle Physics* (Addison-Wesley Publishing Company, Inc., Reading, Massachusetts, 1964), p. 145. Ph. Salin, Nuovo Cimento **28**, 1294 (1963); G. Ascoli, E. L. Goldwasser, U. E. Kruse, J. Simpson, and W. P. Swanson, in *Proceedings of the Sienna International Conference on Elementary Particles and High-Energy Physics, 1963*, edited by G. Bernardine and G. P. Puppi (Società Italiana di Fisica, Bologna, 1963), Vol. I, p. 485; R. L. Walker, in Proceedings of the Conference on Photon Interactions in the GeV Energy Range, Cambridge, 1963, Vol. 4, p. 1 (unpublished); D. A. McPherson, D. C. Gates, R. W. Kenney, and W. P. Swanson, Phys. Rev. **136**, B1465 (1964).

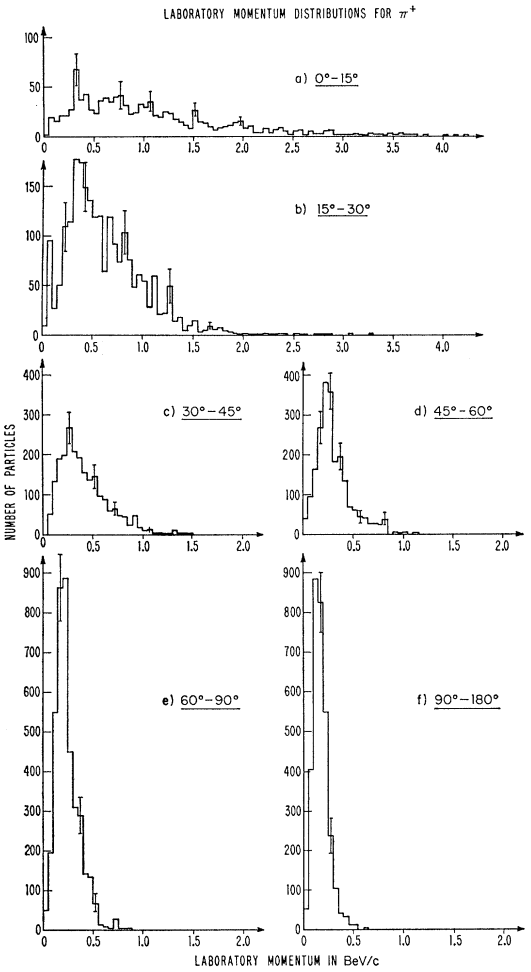

FIG. 14. Laboratory momentum distributions of π^+ in intervals of 50 MeV/c for various regions of π^+ laboratory emission angles.

are produced, as explained in Sec. IV, but only the statistical uncertainties of these subtractions are included in the quoted uncertainties. The systematic uncertainty arising from the method of correction is given in Sec. IV. Not included in these cross sections are 1.6% of the total three-prong events which could not be kinematically fitted, which are included in the unassigned events of Table I.

If an ambiguous event is analyzed as $\gamma p \rightarrow p\pi^+\pi^-\pi^0$, the primary gamma-ray energy calculated will be different (usually 500 MeV/c lower) then if it is analyzed as $\gamma p \rightarrow n\pi^+\pi^+\pi^-$. Hence, the calculated production spectrum of the ambiguous events depends on the assignment made. In order to calculate an upper limit to each reaction cross section, it is necessary to make an assignment for the ambiguous events. For Fig. 9(a), all ambiguous events were assumed to be $\gamma p \rightarrow n\pi^+\pi^+\pi^-$ and a cross section was calculated. The top of the shaded area is the upper limit calculated. Similarily, for Fig. 9(b), all ambiguous events were assumed to be $\gamma p \rightarrow p\pi^+\pi^-\pi^0$ and the top of the shaded area is the upper limit calculated. Note that *no* multiple π^0 correction has been made to the ambiguous events used in the upper-limit calculations.

The central values for the cross sections in Fig. 9 lie in the shaded areas. A reasonable location for this central value is in the center of the shaded area. This center position is consistent with the ratio of the lower limits of the cross sections for the two reactions and the assumption that the $\gamma p \rightarrow n\pi^+\pi^+\pi^-$ reaction will have twice the possibility of confusion as the reaction $\gamma p \rightarrow p\pi^+\pi^-\pi^0$. It is also in agreement with the number of events seen in the ω^0 mass region when all ambiguous events are assumed to be $\gamma p \rightarrow p\pi^+\pi^-\pi^0$ and one plots the invariant mass of the three pions.

Figure 10(a) shows the cross sections for the $\gamma p \rightarrow p\pi^+\pi^+\pi^-\pi^-$ reaction. Figure 10(b) shows the strange-particle cross sections corrected for unseen V^0 decay, due to both the neutral decay modes and to the potential path of the V^0 in the chamber. It also includes corrections for the strange-particle events involving charged K mesons which were missed because the K mesons could not be identified on the basis of bubble density determinations (see Sec. IV). These corrections

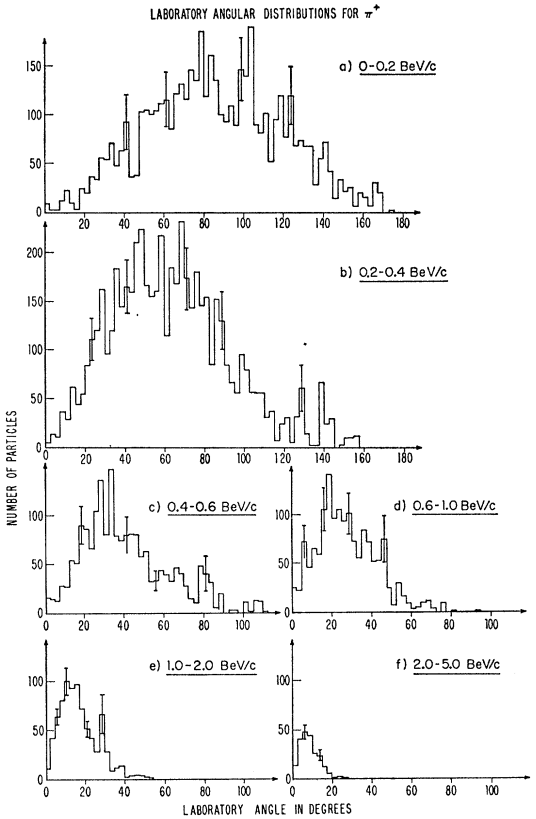

FIG. 15. Laboratory angular distributions of π^+ in intervals of 2.5 deg for various regions of π^+ laboratory momenta.

were calculated using NVERTX[13] for generating the events. Various mechanisms such as

$$\gamma p \to \phi + p \quad \text{and} \quad p \to K^+ + Y^*$$
$$\searrow K^+ + K^- \qquad\qquad \searrow p + K^-$$

yielded results very similar to those obtained assuming Lorentz invariant phase space. Thus these corrections are felt to be good to 10% and this uncertainty is included in the uncertainties given. The 36 ambiguous events in Table I have been included in Fig. 10(b). The contamination from events in which more than the one assumed missing neutral particle is emitted is small since at most 19 such events are involved.

Figure 11 shows the cross section for all events with definite assignments and thus the data points represent a lower limit to the total cross section. These points do not include the single-prong cross sections. The solid line is the cross section for all events (including the single-prong and ambiguous events) with a definite or assumed assignment, as a function of the beam momentum corresponding to that hypothesis.

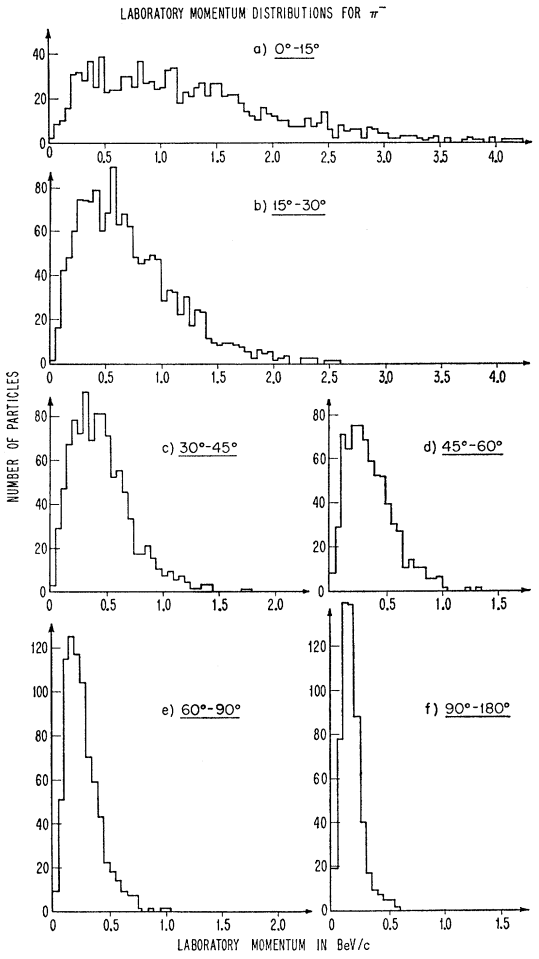

FIG. 16. Laboratory momentum distributions of π^- in intervals of 50 MeV/c for various regions of π^- laboratory emission angles.

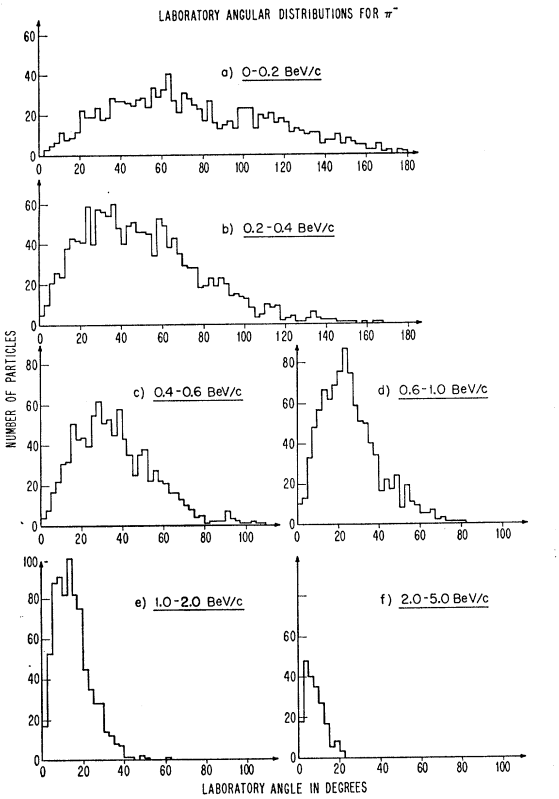

FIG. 17. Laboratory angular distributions of π^- in intervals of 2.5 deg for various regions of π^- laboratory momenta.

For example, all events which were calculated as $\gamma p \to p\pi^+\pi^-\pi^0$ are represented in this curve and thus that fraction of these events which are really $\gamma p \to p\pi^+\pi^-\pi^0\pi^0$ are not given at the correct beam momentum. The same is true of the $p\pi^0$ and $n\pi^+$ events. The only events not included in the solid curve are the unassigned events of Table I (about 1.5% of the total sample) and the seven-prong events.

With the exception of the three-prong, 0C events, the results of this experiment agree within the uncertainties with previous results by Chasan *et al.*[14] and the preliminary results of the Aachen-Berlin-Bonn-Hamburg-Heidelberg-München bubble-chamber collaboration.[10] The difference in the cross section for reactions (4) and (5) between this experiment and that of the latter group is mainly attributable to the correction made for multiple neutral events in this experiment.

[13] C. A. Bordner, Jr., A. E. Brenner, and E. E. Ronat, Rev. Sci. Instr. 37, 36 (1966).

[14] B. M. Chasan, G. Cocconi, V. T. Cocconi, R. M. Schectman, and D. H. White, Phys. Rev. 119, 811 (1960).

VI. LABORATORY DISTRIBUTIONS

Laboratory distributions of the momenta and production angles of charged particles are shown in Figs. 12–17. All events except those including strange particles (2.1% of the total) and unassigned events (1.5% of the total) are included in these figures. The figures show the number of particles produced in a given interval of momentum or angle when a photon flux with the magnitude and energy distribution shown in Fig. 3 is passed through 1.04 g/cm^2 of hydrogen. This incident beam is nearly a bremsstrahlung distribution with a total energy of 2.04×10^8 BeV above 0.1 BeV, which is 3.71×10^7 equivalent quanta if a maximum energy of 5.5 BeV is chosen.

Single-prong events are included in Figs. 12–17 after scaling to the total flux for the rest of the sample.

Particles in the ambiguous events of the 0C multipion sample [reactions (4), (5), (7); and (8) of Table I] are also included; the ambiguous particle is placed in each possible mass category with a weight equal to the fraction predicted by a Monte Carlo calculation using phase-space distributions and applying the experimental criteria to the calculated sample.

The data of Figs. 12–17 are presented for their utility in estimating backgrounds or beam intensities available from photoproduction processes. The recent work done at DESY[15] is in agreement with these results.

ACKNOWLEDGMENTS

We wish to express our deep appreciation to the staff of the Cambridge Electron Accelerator for making the photon beam and the facilities of the CEA available. We wish also to thank our scanning groups for their efficient aid in the analysis of these data. We are indebted to our programming groups for the programming necessary for this experiment.

[15] Aachen-Berlin-Bonn-Hamburg-Heidelberg-München Bubble Chamber Collaboration, DESY 66/34, 1966 (unpublished).

PHYSICAL REVIEW VOLUME 155, NUMBER 5 25 MARCH 1967

π^+ Photoproduction from Hydrogen at Lab Angles from 34° to 155° and Lab Photon Energies from 500 to 1350 MeV*†

HENRY A. THIESSEN‡
California Institute of Technology, Pasadena, California
(Received 17 October 1966)

The differential cross section for the reaction $\gamma+p\rightarrow\pi^++n$ was measured using the Caltech 1.5-GeV electron synchrotron. The positive pions were detected and momentum analyzed in a multichannel magnetic spectrometer and the data were recorded in the memory of a pulse-height analyzer. The energy resolution was improved over previous experiments and an attempt was made to minimize systematic errors. The data are presented in the form of energy distributions at 12 lab angles from 34° to 155°, and the range of lab proton energies extended from 500 to 1350 MeV. Data were not taken at all energies for each angle, since the maximum useful momentum of the spectrometer, 600 MeV/c, restricted the maximum energy for lab angles less than or equal to 74°.

I. INTRODUCTION

THERE is presently considerable theoretical interest in photoproduction data, in part because of their importance in the evaluation of sum rules derived from the algebra of current components.[1–3] For these purposes, a detailed multipole and isotopic-spin decomposition of the photoproduction amplitudes is required. A phenomenological decomposition can be significant only if accurate and extensive data on differential cross sections are available, supplemented by data on recoil-nucleon polarization and polarized incident-photon asymmetries.

This paper reports the results of an experiment which was designed to measure the cross section for the reaction $\gamma+p\rightarrow\pi^++n$ at a large number of points with a minimum of systematic errors and good energy resolution. Measurements were made at pion lab angles from 34° to 155° and photon lab energies from 500 to 1350 MeV. The energy range was chosen to include the region in which the following resonant pion-nucleon states are important: $P_{11}(1400)$, $D_{13}(1518)$, $S_{11}(1550)$, $D_{15}(1688)$, and $F_{15}(1688)$.[4] Additional experiments and a phenomenological analysis of all existing data are in

* Work supported in part by the U. S. Atomic Energy Commission. Prepared under Contract No. AT(11-1)-68 for the San Francisco Operations Office, U. S. Atomic Energy Commission.

† This work is submitted in partial fulfillment of the requirements for the degree of Doctor of Philosophy at the California Institute of Technology.

‡ Present address: Los Alamos Scientific Laboratory, University of California, Los Alamos, New Mexico.

[1] A. Bietti, Phys. Rev. **142**, 1258 (1966).
[2] A. Bietti, Phys. Rev. **144**, 1289 (1966).
[3] F. Gilman and H. Schnitzer, Phys. Rev. **150**, 1362 (1966).
[4] P. Bareyere, C. Brickman, A. V. Stirling, and G. Villet, Phys. Letters **19**, 342 (1965).